AIAA JOURNAL
Vol. 43, No. 11, November 2005

Effect of Geometric Scaling on Aerodynamic Performance

R. Grimes,* E. Walsh,* D. Quin,† and M. Davies‡
University of Limerick, Limerick, Ireland

Miniaturization of modern electronics and simultaneous elevation in heat dissipation means that future compact electronic systems are likely to be too hot to be held in the users hand. As a result, novel compact cooling technologies are required. In systems such as mobile phones and palmtop computers, macroscale fans cannot be used to overcome this problem because they are too large. As a solution, the implementation of microfan technology is proposed. Aerodynamic scaling issues in microaxial flow fans are addressed. Analysis shows how reduction of fan dimensions to the microscale causes increased local loss. Numerical simulations were performed to investigate the validity of the scaling theory, the results of which give confidence in the scaling analysis. Measurements were carried out on two geometrically similar fans to validate the theory under experimental conditions. Results of these measurements were in good agreement with the analysis. The fundamental finding is that a reduction in scale is accompanied by a reduction in efficiency and, thus, fan performance. It is concluded that geometric scaling alone of macroscale designs is not sufficient to produce microscale cooling fans: Modifications must be made to the geometry that account for changes in flow physics.

Nomenclature

A	=	flow area, m^2
C	=	variable constant
C_d	=	nondimensional entropy, $TS''/\rho U_e^3$
c	=	mean fan airspeed, m/s
D	=	fan diameter, m
F	=	force, N
K	=	acceleration parameter, $(\theta^2/\upsilon)(\mathrm{d}U_e/\mathrm{d}x)$
$\dot{m}$	=	mass flow rate, m^3/s
P	=	pressure, Pa
P_r	=	pressure ratio
P_{static}	=	static pressure, Pa
P_{total}	=	total pressure, Pa
Q	=	volumetric flow rate, kg/s
R	=	gas constant, J/kg · K
Re_x	=	Reynolds number, $U_e x/\upsilon$
Re_θ	=	Reynolds number, $U_e\theta/\upsilon$
r	=	fan radius, m
S	=	specific entropy, J/kg · K
S'	=	entropy generation rate per unit length, W/m · K
S''	=	entropy generation rate per unit area, $W/m^2 \cdot K$
T	=	temperature, K
U	=	local velocity, m/s
V	=	local airspeed at fan outlet, m/s
W	=	work, J
x	=	scale factor
y	=	perpendicular distance from wall, m
β	=	fan blade trailing-edge angle, rad
δ	=	boundary-layer thickness, m
δ_3	=	energy thickness, m
δ^*	=	displacement thickness, m
η	=	efficiency, %
θ	=	momentum thickness, m
μ	=	dynamic viscosity, kg/ms
ρ	=	density, kg/m^3
υ	=	kinematic viscosity, m^2/s
ω	=	angular velocity, rad/s

Subscripts and Superscripts

a	=	axial componet
actual	=	measured quantity
b	=	blade value
e	=	conditions at boundary-layer edge
isen	=	isentropic conditions
r	=	radial component
root	=	blade root conditions
s	=	static quantity
T	=	tangential component
t	=	total quantity
tip	=	blade tip conditions
1	=	conditions at fan inlet
2	=	conditions at fan outlet

Received 14 October 2004; revision received 13 May 2005; accepted for publication 20 May 2005.

*Senior Research Fellow, Stokes Research Institute, Department of Mechanical and Aeronautical Engineering.

†Postgraduate Student, Stokes Research Institute, Department of Mechanical and Aeronautical Engineering.

‡Professor in Engineering Science, Stokes Research Institute, Department of Mechanical and Aeronautical Engineering.

I. Introduction

BECAUSE of consumer demands for smaller, more functional products, heat flux densities in many portable electronic devices are growing. Unless technologies are developed to remove this heat at acceptable temperatures, the implications on future generations of products such as mobile telephones and palmtop computers will be twofold. First, component reliability will be reduced. Second, and perhaps more important, case temperatures will be elevated to the extent that will prohibit a user from handling the device. With the use of current passive cooling methodologies, it is believed that these thermal issues will be the primary constraint to the full implementation of many technologies currently under development for a range of portable electronic devices.[1]

A number of technologies are under development for thermal management of portable electronic devices, including piezoelectric fans,[2] phase-change materials,[3] and micro heat pipes.[4] Each technology has been shown to have its own benefits and complications. What is clear from the cited literature is that it will most likely be a combination of a number of current technologies that will cool the next generation of high-power density portable electronics. It is envisaged that microaxial flow fans, the focus of this paper, will be key components in this combination of technologies because they have the potential to remove heat from critical components and exhaust it to the ambient in a relatively simple and effective manner. Indeed in high-power density nonportable electronics, this has been the norm

for a number of years when macroscale fans have been used. Current issues with the development of microscale fans are difficulty of manufacture and lack of knowledge about fan aerodynamic performance on the microscale. This paper addresses the latter, the effect of scaling on the aerodynamic performance of electronic cooling fans. Understanding of this is a fundamental component in the design of microfans for use in future electronic systems.

The differences in the performance of the micro- and macroscale fans originate from a number of different flow phenomena. Perhaps the most important aspect of a scaling analysis is to elucidate the point at which one's understanding of the loss mechanisms as gained from conventional macrofans is no longer valid. In this paper, the effects of scaling on the dominant loss mechanisms are addressed in terms of entropy production, thus allowing a direct comparison between different sources of loss irrespective of their origin. The effects of scaling on the flow regime in micropassages is also addressed to identify where the loss mechanisms from the macroscale change in the microscale for a given geometry.

A numerical analysis, using a commercial package FLUENT 5 was performed to aid in the understanding of the flow in micropassages and to compare with the scaling analysis. To investigate experimentally the scaling of fan loss, a commercially available 0.12-m-diam fan was used as a datum and a geometrically scaled model of this fan was fabricated. The datum fan is typical of those used in cooling electronic systems. The scale model was one-third the size of the datum fan and was fabricated by using traditional computer numerical control machining techniques. The relatively simple theory developed is found to agree well with both the computational fluid dynamics (CFD) prediction and the experimental measurements. The authors are currently performing an experimental investigation of flow in a 1/20-scale model of the datum fan, and initial results suggest that the theory can be extended quite accurately to this smaller-scale fan.

II. Theory

Numerous investigators, including Grimes,[5] have shown that the performance of fans is governed by four nondimensional groups: pressure ratio, mass flow number, specific speed, and Reynolds number. For larger-scale fans, operating at high Reynolds numbers, with turbulent boundary layers, the effects of Reynolds number on performance are small. In such instances, the performance is commonly presented as in Fig. 1, where mass flow number is plotted against pressure ratio for a range of specific speeds. Here, the performance of all geometrically similar fans, operated at the same specific speed, should collapse onto a single curve, regardless of Reynolds number. However, as will be discussed in the next section, as the Reynolds number is reduced and boundary layers become laminar, the efficiency of the fan becomes particularly sensitive to Reynolds number. To operate fans of varying scale at constant specific speed, the linear blade tip speed is kept constant. Therefore, the only Reynolds number parameter that varies is the characteristic length, and so Reynolds number is proportional to fan scale. Varying fan speed with scale in this manner is typical in electronics cooling applications, where fans are operated at an acoustically imposed limiting speed.

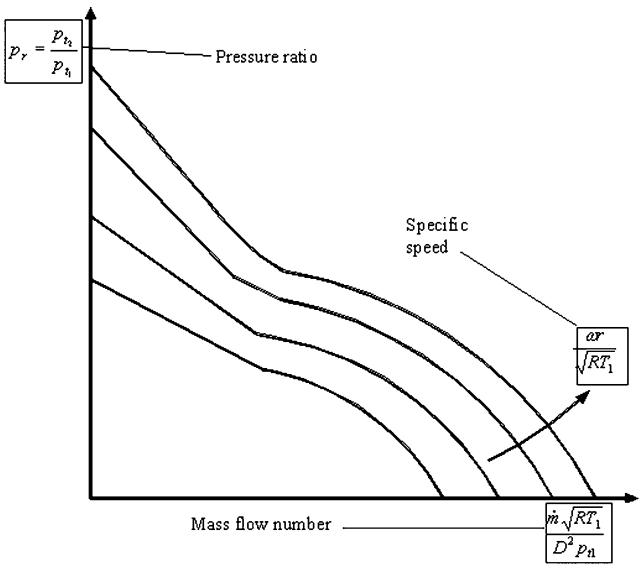

Fig. 1 Nondimensional fan performance.

Reduction in fan size results in a reduction in efficiency and a change in fan performance. This is a critical factor in the design of micro cooling fans and is caused by a relative increase in entropy production. To demonstrate this, consider the nondimensional entropy production rate per unit area in laminar boundary layers, which is given as[6]

$$C_d = 0.17 Re_\theta^{-1} \tag{1}$$

This equation is derived from the well-known Pohlhausen family of velocity profiles.[7] In Eq. (1), the scale that is altered by geometric size is the momentum thickness, which is given by[8]

$$\theta = 0.664x \Big/ \sqrt{Re_x} \tag{2}$$

Hence, the entropy production rate per unit area in a laminar boundary layer scales as $1/\sqrt{x}$. Therefore, the entropy production rate per unit area at a fixed nondimensional distance along a wetted surface would increase inversely with the square root of the reducing length scale. Thus, 1/3-, 1/20-, and 1/100-scaled fan geometries would have increases in local entropy generation rates of 1.73, 4.47, and 10, respectively, at a given nondimensional distance. With use of the same approach, Table 1 shows the effect of scaling on the various sources of entropy production, where they are also compared to the relevant scaling in the macrorange.

The state of the boundary layer, that is, laminar, transitional, or turbulent, is heavily dependent on the Reynolds number of the flow. At high Reynolds numbers where turbulent boundary layers dominate, the entropy generation rate in the boundary layers is only weakly dependent on the length scale as seen from Table 1. However, in the case of small/microlength scales, where laminar flow will unquestionably dominate, there is a large increase in the local entropy generation rate in the boundary layer as shown in Table 1. Effectively, for a fixed percentage chord location, the entropy generation will be an order of magnitude higher, whereas the local Reynolds number will be two orders of magnitude lower for the 1/100-scale fan.

This is an unfortunate phenomenon because it results in both a reduction in efficiency and performance of the microfan. When the analysis of Denton[9] is applied, the entropy generated behind the trailing edge is dependent on the state of the boundary layer at the trailing edge and, thus, scales similarly to the boundary layers. When the typical shape factors given in Table 1 are used, it may be deduced that for a turbulent boundary layer approximately 15% of the total entropy is generated behind the trailing edge, whereas for a laminar boundary layer this figure increases to approximately 25%. The state of the boundary layer and the changing contribution of different loss mechanisms to the total entropy production are key changes that occur on the microscale. The scaling of the blockage caused by the boundary layer is also shown in Table 1, where it is found to be much more significant in laminar than turbulent boundary layers. This increased blockage adds directly to the entropy production, but more important is its indirect effect on the entropy production because it may change the boundary-layer edge velocity distribution and, thus, fundamentally change ones understanding of the flowfield. Indeed if this effect is large, then much of the scaling analysis is invalidated because more parameters than the length scale are being varied.

There are a number of other loss mechanisms including boundary-layer transition, boundary-layer separation, end wall losses, and leakage losses, which are known to generate a large proportion of the overall loss. However, no relationship has been derived to show the effect of scaling on these loss mechanisms. This is due to the extreme complexity of the flow in these regions. Because these losses

Table 1 Effects of scaling on sources of fan entropy production

Parameter	Equation	Equation used to scale	Scale factor	$X=0.33$	$X=0.05$	$X=0.01$
Reynolds number	$Re_x=\rho u x/\mu$	——	x	0.33	0.05	0.01
Entropy generation rate per unit area in turbulent boundary layer	$C_d=0.0056Re_\theta^{-1/6}$ (Schlichting[8])	$\theta=0.0156x/Re_x^{1/7}$ (White[12])	$1/x^{1/7}$	1.17	1.53	1.93
Entropy generation rate per unit area in laminar boundary layer	$C_d=0.17Re_\theta^{-1}$ (Truckenbrodt[6])	$\theta=0.664x/Re_x^{1/2}$ (Schlichting[8])	$1/x^{1/2}$	1.73	4.47	10
Percentage of total entropy generated behind trailing edge in turbulent boundary layers	$S'_{\text{wake}}=\rho U_e^3(2\theta-\delta_3)/2T$ (Denton[9])	$\delta_3/\theta=1.7$ (Schlichting[8])	$C\approx 15\%$	——	——	——
Percentage of total entropy generated behind trailing edge in laminar boundary layers	$S'_{\text{wake}}=\rho U_e^3(2\theta-\delta_3)/2T$ (Denton[9])	$\delta_3/\theta=1.57$ (Pohlhausen[7])	$C\approx 25\%$	——	——	——
Blockage in turbulent boundary layers: displacement thickness/passage width	δ^*/PW	$\delta^*=0.02x/Re_x^{1/7}$ (White[12])	$1/x^{1/7}$	1.17	1.53	1.93
Blockage in laminar boundary layer: displacement thickness/passage width	δ^*/PW	$\delta^*=1.72x/Re_x^{1/2}$ (Schlichting[8])	$1/x^{1/2}$	1.73	4.47	10
Separation criteria	$K=(\theta^2/\upsilon)(\mathrm{d}U_e/\mathrm{d}x)$ (Thwaites[10])	$\theta=0.664x/Re_x^{1/2}$ (Schlichting[8])	C	——	——	——
Centripetal force	$F=mr\omega^2$	$m=\rho r\,\mathrm{d}\theta\,\mathrm{d}r\,\mathrm{d}z$ (Hill and Peterson[13])	C	——	——	——
Efficiency	$\eta=1-TS_{\text{gen}}/W_{\text{isentropic}}$	$1-\eta=TS_{\text{gen}}/W_{\text{isentropic}}$	$1/x^{1/2}$	1.73	4.47	10

are predominately of a viscous and mixing nature similar to that found in boundary layers and wakes, here it will be assumed that the local entropy production will increase with decreasing length scale in analogy with the boundary layer and wake losses. When this rather gross assumption is made, a scaling for the efficiency of microfans is deduced from Table 1 by using

$$1-\eta=TS_{\text{gen}}/W_{\text{isentropic}} \tag{3}$$

the entropy generation rate per unit area in a laminar boundary layer scaled inversely with the square root of the length scale. Therefore, the total entropy generation rate scales with the length scale to the power of 1.5 and the isentropic work scales with the length scale squared, yielding

$$(1-\eta_x)\sqrt{x}=(TS_{\text{gen}}/W_{\text{isentropic}})_{\text{datum}} \tag{4}$$

Thus, for 1/3-, 1/20-, and 1/100-scaled fans, Eq. (4) would yield a prediction for the increase in total entropy generation rates relative to isentropic work of 1.73, 4.47, and 10, respectively. The general equation for the reduced efficiency may be expressed as

$$\eta_x=1-\underbrace{\left[\left(1/\sqrt{x}\right)\underbrace{(1-\eta_{\text{datum}})}_{\text{datum.fan.loss}}\right]}_{\text{scaled.fan.loss}} \tag{5}$$

As suggested by Eq. (5), reduced scale increases the relative entropy produced by the fan. If the scale is reduced excessively, then the entropy produced exceeds the pressure rise generated and the work done by the fan becomes zero. At this scale, the efficiency is zero. Numerical predictions and calculations of isentropic pressure rise have shown this limiting case to be at a scale of approximately 1/200 of the datum fan for the operating point modeled.

As noted earlier, blockage indirectly affects the entropy production by changing the flow regime through a passage; other flow phenomena such as separation and centripetal forces may also affect the flow regime to alter one's understanding of the loss mechanisms. Therefore, the effect of scaling on these parameters needs to be addressed. When boundary-layer transition is neglected, which is extremely unlikely on the microscale, the effect of scaling on boundary-layer separation is shown in Table 1 to be independent of scale for laminar boundary layers by considering the separation criteria of Thwaites.[10] However, other separation criteria do exist, which show an earlier separation with decreasing scale.[11] The effects of scaling on the centripetal forces are also shown to be independent of scale in Table 1. The independence of these parameters on scale is important and gives some confidence in the use of the described scaling parameters in the mini/microregime of fan design.

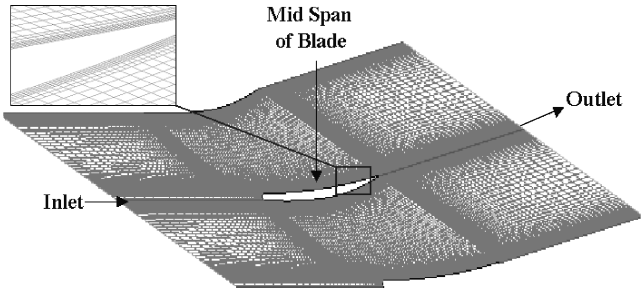

Fig. 2 Numerical model of flow-through fan blade passage.

III. Numerical Models

Initially, data from a commercially available CFD code, FLUENT 5, using a laminar solver was compared with the scaling analysis presented in the scaling section. A two-dimensional unstructured grid was constructed that modeled the flow at the midspan in a passageway of the fan. The model consisted of 11,500 cells, where grid independence was checked by doubling the number of cells. Cyclic boundary conditions were applied to model an infinite cascade. Figure 2 shows the grid used to model the flowfield, with the unstructured grid allowing a high density of cells to exist in the near-wall region, which resulted in good definition of the boundary layer. Four models were run with scale factors of 1, 1/3, 1/20, and 1/100, corresponding to inlet Reynolds number based on chord of 5×10^4, 1.6677×10^4, 2.5×10^3, and 500, respectively. The models were then used to compare with the scaling analysis presented earlier and to aid in the understanding of the fluid flow. The analyses were done with fixed blade shape and inlet flow properties. A constant inlet velocity of 13.65 m/s was specified at zero incidence to the leading edge. This corresponds to the boundary conditions at blade midspan, in the middle of the fan's recommended operating range. Figure 3 shows the resultant data from the CFD as calculated points. Curve fits are included to represent the scaling analysis of Table 1 (Refs. 6, 8–10, 12, and 13). The data points for the entropy generation rate per unit area and the blockage were obtained by extracting the boundary-layer velocity profiles at the trailing edge of the pressure surface and calculating the entropy generation rate per unit area and blockage taking into consideration pulse width (PW) by using Eqs. (6) and (7), respectively. The total entropy is calculated by extracting the total pressure at the outlet and inlet from the CFD solution and using Eq. (8) to give the specific entropy, which is then multiplied by the mass flow rate to obtain the total entropy

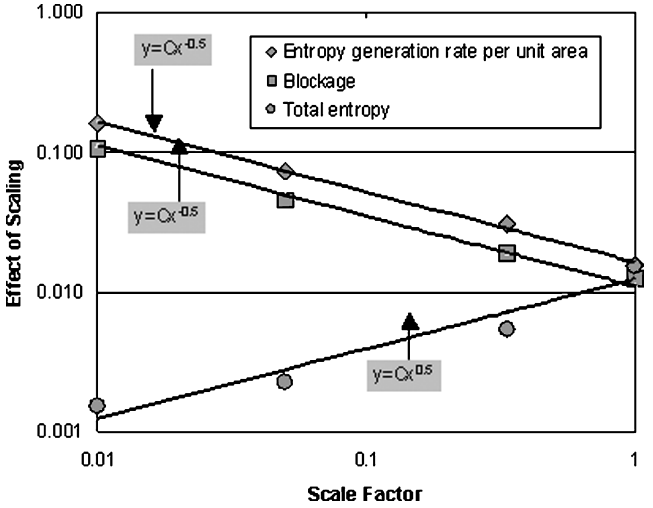

Fig. 3 Comparison of CFD results and scaling analysis from Table 1.

generation rate predicted by the model,

$$S'' = \int_0^{\delta} \frac{\mu}{T}\left(\frac{\partial u}{\partial y}\right)^2 \mathrm{d}y \tag{6}$$

$$\text{blockage} = \frac{\int_0^{\delta} 1 - (u/U_e)\,\mathrm{d}y}{\mathrm{PW}} \tag{7}$$

$$\Delta S = -R\,\ell_n\left(\frac{P_{t2}}{P_{t1}}\right) \tag{8}$$

From Fig. 3, it is seen that the predicted local entropy generation rate and the blockage agree very well with the scaling analysis because both are shown to scale as detailed in Table 1. This result must be taken with caution because the complicated aerodynamic mechanisms of a realistic three-dimensional flow can never be modeled in such a simple two-dimensional way. To this end, an experimental investigation was undertaken to determine the validity of the scaling analysis under realistic operating conditions.

IV. Experimental Techniques and Data Reduction

Tests were performed with a datum 120-mm-diam fan and a geometrically similar one-third-scale model of the datum fan. This section describes the facilities used to perform pressure flow characterization and detailed velocity distribution measurements on these fans. The operating Reynolds numbers based on the midspan chord length of these fans correspond with the Reynolds numbers for the numerical analysis presented in the preceding section.

The test facility shown in Fig. 4 measured the performance of the one-third-scale fan. A separate test facility is built for each scale fan to reduce the effects of any inherent rig leakage on the resultant fan characteristic. All facilities were built in accordance with British Standard BS 848 (Ref. 14). Air enters the test facility through the orifice plate, which measures the flow rate. The relationship between flow rate and pressure drop was determined previously by calibration experiments.[15] Air then passes the pipe section. The straightening vane removes any swirl. Variation of auxiliary fan speed changes the operating point of the test fan. Another straightening vane removes any swirl before the air enters the fan inlet chamber. Screens of 60, 50, and 45% open area ensure uniform velocity in the air passing the fan inlet pressure tappings. The air exits the test facility through the test fan. The static pressure rise across the test fan is measured using a manometer connected to the fan inlet pressure tappings and to the atmosphere.

A. Particle Image Velocimetry Measurement of Velocity Distribution

Velocity field tests were carried out using particle image velocimetry (PIV). The test fan was held in a characteristic test facility

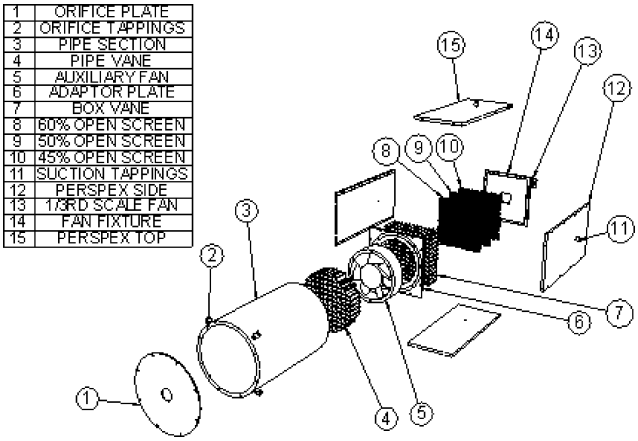

Fig. 4 Fan characteristic test facility.

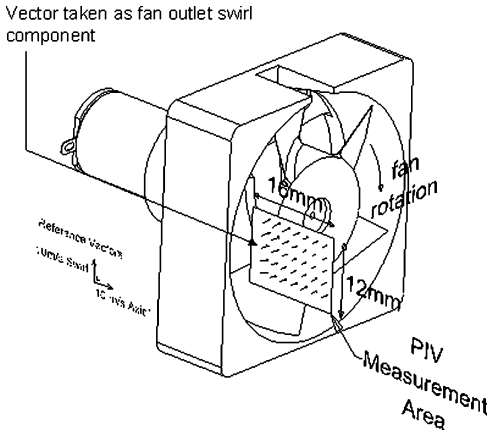

Fig. 5 Axial and swirl measurement area on one-third-scale fan; measurement plane set at blade midspan (14.5 mm radius). Fan operating at 0-Pa static pressure rise, 8400 rpm; only 1 in 25 of the measured PIV vectors shown.

to set and measure the pressure rise. The flow through the test fan was seeded with smoke. A New Wave Research Nd YAG Minilaser generated a light sheet and illuminated the seeding particles passing through the fan. An 80C42 Double Image 700 camera was focused on a region of this illuminated plane of smoke. When images in rapid succession were compared a Dantec PIV Flowmap 2100 Processor calculated all velocities in the flowfield. Calibration tests[16] on the PIV system have shown an average accuracy of 3.8% for three-dimensional flows of this type.

The swirl velocity component was measured by radially moving the measurement plane shown in Fig. 5 across the blade span, in 2- and 1-mm increments, respectively, for the datum and one-third-scale fans. As shown in Fig. 5, the swirl component of velocity was taken as the center vector in the upstream column of vectors of the vector array for each measurement field. As stated earlier, PIV measurements of the 1/20-scale fan are currently underway.

The measurement plane shown in Fig. 6, used for the measurement of axial and radial velocity components, was positioned as near to the blade trailing edge as possible. The field of view consisted of 768×484 pixels and 47×29 interrogation areas, each of which had $50 \times 50\%$ overlap. The field of view was zoomed in to maximize measurement resolution in the area of interest. The measurement area could not be positioned too closely to the trailing edge of the fan blades because of laser reflection. For the datum fan, a 6-mm offset was necessary and for the one-third-scale fan a 2-mm offset.

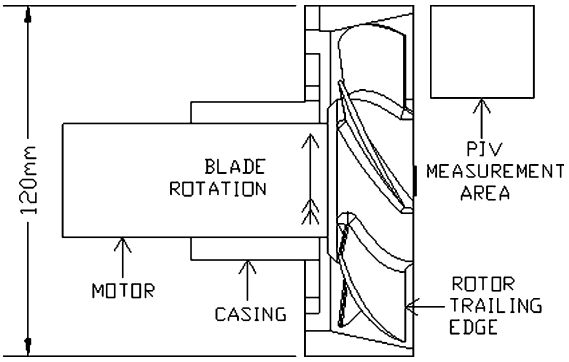

Fig. 6 Outlet measurement area for axial and radial PIV measurements on datum fan.

B. Data Reduction

The actual fan efficiency was calculated from measured fan performance and blade geometry. The blade was analyzed using velocity triangles to give the isentropic fan pressure rise and the isentropic work done by the fan given by

$$P_{\text{isen}} = \int_{\text{root}}^{\text{tip}} \rho \left(V_b - \frac{V_a}{\tan \beta} \right) V_b \, \mathrm{d}A \Big/ A \tag{9}$$

$$\dot{W}_{\text{isen}} = P_{\text{isen}} Q \tag{10}$$

The local airspeed at the fan outlet is derived from PIV readings using

$$V = \sqrt{V_a^2 + V_r^2 + V_T^2} \tag{11}$$

The mean velocity at the fan outlet is determined by the flow rate weighted kinetic energy function

$$c_2 = \sqrt{\frac{\int_{\text{root}}^{\text{tip}} \left(V^2 V_a r \right) \mathrm{d}r}{\int_{\text{root}}^{\text{tip}} \left(V_a r \right) \mathrm{d}r}} \tag{12}$$

Total pressure rise across the fan was calculated from measurements with Eq. (13) and used to calculate the subsequent actual work done by the fan through Eq. (14) and actual fan efficiency by using Eq. (15). Thus,

$$P_{\text{total}} = P_{\text{static}} + \tfrac{1}{2} \rho \left(c_2^2 - c_1^2 \right) \tag{13}$$

$$\dot{W}_{\text{actual}} = P_{\text{total}} Q \tag{14}$$

$$\eta = \dot{W}_{\text{actual}} / \dot{W}_{\text{isen}} \tag{15}$$

V. Results and Discussion

The measured pressure flow characteristics for the datum and one-third-scale fans are shown in Fig. 7. As can be seen, the static pressure characteristics for both fans match quite closely. However, because the measured velocity magnitude at outlet from the one-third-scale fan was less than that measured for the datum fan, the total pressure characteristic for the one-third-scale fan falls below the datum fan total pressure characteristic. As a result, the measured efficiency for the one-third-scale fan falls below that of the datum fan, as shown in Fig. 8. Also shown in Fig. 8 is a prediction of the one-third-scale fan efficiency, calculated from the measured datum fan efficiency, by using Eq. (5). The agreement is reasonably good, thus, giving some confidence in the scaling analysis despite the over simplification of the loss mechanisms in such a device. Further work is required before such a model could be applied confidently to a range of scales and fan geometries. To this end, the authors are investigating a 1/20-scale model of the same geometry. From an electronic cooling perspective, the large drop in efficiency with reducing scale is of great concern and seems to indicate that a simple geometric scaledown of current fan design will not suffice. Novel aerodynamic designs are required to overcome the adverse scaling phenomena that are encountered.

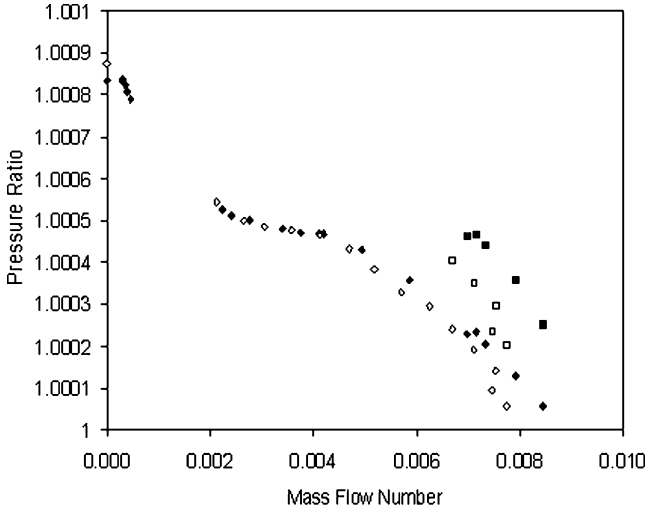

Fig. 7 Datum and one-third scale fan characteristics; specific speed of both fans was 0.061: ■, datum total; □, 1/3 scale total; ◆, datum static; and ◇, 1/3 scale static.

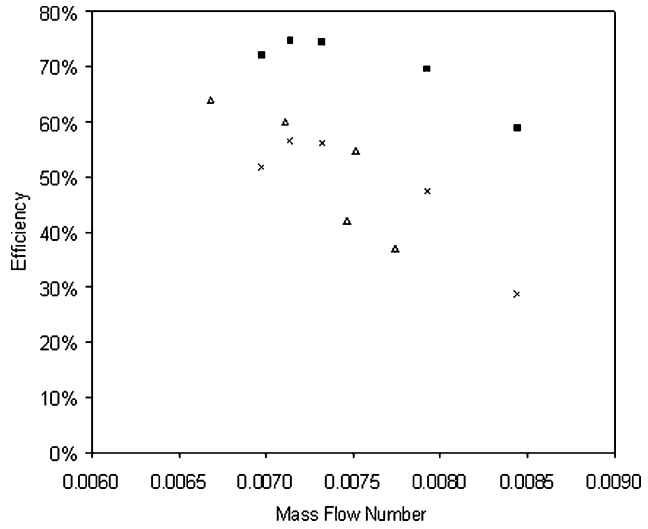

Fig. 8 Measured and predicted efficiencies of datum and one-third-scale fans operating at specific speed of 0.061: ■, datum measured; △, 1/3 scale measured; and ×, 1/3 scale, predicted from datum measurements by using Eq. (1).

VI. Conclusions

A scaling analysis has been developed in an attempt to predict the efficiency of fans with reducing scale. The two-dimensional predictions and the experimental measurements agree reasonably well with the scaling analysis. Much further experimental work is required on both varying geometries and scales before such a simple prediction method can be put into widespread use. The implications of this work for electronic cooling suggest that fan redesign rather than simply scaling may be in order before the technology becomes more commercially viable.

Acknowledgments

The authors gratefully acknowledge Enterprise Ireland and Irish Research Council for Science, Engineering and Technology for their financial support and the technical staff of the University of Limerick.

References

[1]International Technology Roadmap for Semiconductors 2003 Edition, *Assembly and Packaging*, Semiconductor Industry Association, 2003, http://public.itrs.net/Files/2003ITRS/Home2003.htm [cited 22 May 2004].

[2]Yoo, J.-H., Il, J., and Cao, W., "Piezoelectric Ceramic Bimorph Coupled to Thin Metal Plate as Cooling Fan for Electronic Devices," *Sensors and Actuators A: Physical*, Vol. 79, No. 1, 2000, pp. 8–12.

[3]Tan, F. L., and Tso, C. P., "Cooling of Mobile Electronic Devices Using Phase Change Materials" *Applied Thermal Engineering*, Vol. 24, No. 2–3, 2004, pp. 159–169.

[4]Launay, S., Sartre, V., and Lallemand, M., "Experimental Study on Silicon Micro-Heat Pipe Arrays," *Applied Thermal Engineering*, Vol. 24, No. 2–3, 2004, pp. 233–243.

[5]Grimes, R., "On Air Flow and Heat Transfer in Fan Cooled Electronic Systems," Ph.D. Dissertation, Mechanical and Aeronautical Engineering Dept., Univ. of Limerick, Limerick, Ireland, June 2001.

[6]Truckenbrodt, E., "An Approximate Method for the Calculation of the Laminar and Turbulent Boundary Layer by Simple Quadrature for Two-Dimensional and Axially Symmetric Flow," *Journal of Aeronautical Science*, Vol. 19, June 1952, pp. 428, 429.

[7]Pohlhausen, K., "Zur näherungsweisen Integration der Differentialgleichung der laminaren Reibungsschicht," *ZAMM*, Vol. 1, Aug. 1921, pp. 252–268.

[8]Schlichting, H., *Boundary Layer Theory*, 6th ed., McGraw–Hill, New York, 1968, pp. 131, 192, 635, 653.

[9]Denton, J. D., "Loss Mechanisms in Turbomachines," *Journal of Turbomachinery*, Vol. 115, Oct. 1993, pp. 621–656.

[10]Thwaites, B., "Approximate Calculation of the Laminar Boundary Layer," *Aeronautical Quarterly*, Vol. 1, 1949, pp. 245–280.

[11]Mayle, R. E., "The Role of Laminar-Turbulent Transition in Gas Turbine Engines," *Journal of Turbomachinery*, Vol. 113, Oct. 1991, pp. 509–537.

[12]White, F. M., *Fluid Mechanics*, 3rd ed., McGraw–Hill, New York, 1994, pp. 400–405.

[13]Hill, P., and Peterson, C., *Mechanics and Thermodynamics of Propulsion*, 2nd ed., Addison Wesley, Reading, MA, 1992, pp. 332–336.

[14]British Standard BS 848: Fans for General Purposes, Part 1: Methods for Testing Performance, British Standards Institution, London, 1980.

[15]Grimes, R., Walsh, E., Kunz, S., Davies, M., and Quin, D., "Scaling the performance of Micro-fans," First International Conf. on Microchannels and Minichannels, American Society of Mechanical Engineers, ICMM2003-1118, April 2003.

[16]Grimes, R., and Davies, M., "Aerodynamic and Thermal Investigation into Axial Flow Fan Cooling of Electronic Systems, Part 1: Measurement Techniques and Steady Flow Measurements," 35th National Heat Transfer Conf., American Society of Mechanical Engineers, NHTC01-14110, June 2001.

C. Kaplan
Associate Editor